

Plastic Deformation and Interfacial Sliding in Al and Cu Thin Film : Si Substrate Systems Due to Thermal Cycling

I. Dutta, M.W. Chen*, K. Peterson and T. Shultz

*Center for Materials Science and Engineering
Department of Mechanical Engineering
Naval Postgraduate School
Monterey, CA 93943*

** Department of Mechanical Engineering
Johns Hopkins University
Baltimore, MD.*

Abstract

As a result of the large difference in thermal expansion coefficients between metal and Si, high stresses can develop in thin metallic films attached to Si substrates in micro-electronic devices during thermal excursions experienced in processing steps or service. These stresses may induce plastic deformation of the thin films accompanied by creep and interfacial sliding, and have a pronounced effect on the reliability of microelectronic devices and components. Even though various methods have been proposed to study thermal stress, methodologies for studying plastic deformation of thin films are not well-established. Here, we report the results of a study of plastic deformation and interfacial sliding of thin Al and Cu films on Si substrates during thermal cycling. Cross-sectional profiles of pattern-grown Al and Cu films of nominally 250nm thickness were measured before and after thermal cycling by employing an atomic force microscope (AFM). Through statistical analysis, the size changes of the thin films induced by thermal cycling were determined. Finite element (FE) analyses were conducted to compute the stress and strain states within the thin film and at the interface, and the results were utilized to interpret the AFM observations. Experiments revealed that following thermal cycling, Al films *expanded* relative to the Si substrate, whereas Cu films *shrank*, resulting in an alteration of the film-footprint on the substrate in both cases. Based on the FE calculations, this was attributed to net inelastic deformation of the thin films via creep and yielding, with the deformation being accommodated at the interface by diffusion-controlled interfacial sliding.

1. Introduction

The mechanical behavior of thin films on semiconductor substrates are of much interest to the microelectronics industry. Thin films generally have properties different from their bulk counterparts, and their thermo-mechanical response may be influenced significantly by the underlying substrate [1,2]. Due to differences in the coefficient of thermal expansion (CTE) between thin metallic films and semiconductor substrates in microelectronic devices, large stresses can develop in thin films during thermal excursions experienced in processing steps or service. This may induce plastic deformation of the thin films accompanied by creep and interfacial sliding [3-5], possibly leading to a pronounced effect on the reliability of microelectronic devices and components.

During thermal cycling, a metallic film attached to a substrate traverses through a range of stress/temperature regimes, leading to the operation of a multitude of plastic deformation mechanisms, such as dislocation glide (i.e., yielding), as well as dislocation and diffusional creep [3,4]. In the absence of interfacial sliding, this plasticity results in stress relaxation in the film, with no relative size change between the film and the substrate. However, if interfacial sliding is allowed to occur, plastic deformation

of the film may be accommodated by differential deformation between the film and the substrate, resulting in a change of the film size.

Recently, Chen and Dutta [5] studied deformation of unpassivated, small-area Al thin films on Si substrates by atomic force microscopy (AFM), and noted significant changes in film-dimensions associated with thermal cycling. This was attributed to plastic deformation of the film, accommodated by diffusion-controlled interfacial sliding near the film-edges, which allowed the lateral dimensions of the film to change. It was suggested [5] that the impact of sliding, and hence the proportionate change in film size, increases with decreasing film width. Since the current trend in microelectronics is towards progressively smaller line widths, it is likely that such effects will assume considerable importance in future devices, making it important to develop an understanding of the roles of film plasticity and interfacial sliding in thin film systems.

In this paper, we report on the results of a study of plastic deformation of Al and Cu thin films on Si substrates using AFM and finite element modeling (FEM), with the goal of understanding the effects of film plasticity and interfacial deformation on the dimensional stability of thin films.

2. Background

It has been demonstrated theoretically and experimentally that the deformation of one of the phases in a multi-component system may be accommodated at the interface by interfacial creep, resulting in dimensional differences between the components during thermo-mechanical loading [6,7]. In fiber-reinforced metal-matrix composites, for instance, interfacial sliding has been observed near fiber-ends during thermal cycling, resulting in a difference between the lengths of the fiber and matrix phases, although they were identical in length prior to cycling [7,8]. This differential deformation has been attributed to plasticity/creep of the metallic-matrix due to internal residual stresses, accommodated by interfacial sliding near the fiber-ends. Experiments on high-density Cu/Ta/Polyimide interconnect structures deposited on a Si wafer have also shown evidence of interfacial sliding between Cu lines and Ta liners, resulting in the appearance of out-of-plane steps on an initially smooth surface following thermal cycling corresponding to dielectric processing conditions [9]. In both cases, interfacial sliding was thought to occur by a diffusional mechanism, driven by interfacial shear stresses generated due to thermal expansion mismatch between the constituent phases (in the axial direction for matrix and fiber, and out-of-plane direction for Cu and polyimide).

Funn and Dutta [10] have shown that interfacial sliding in the absence of adhesive failure may be described by a diffusional creep law with a threshold stress and an activation energy corresponding to interfacial diffusion. Based on a periodic interface model, they proposed that sliding occurs by interface-diffusion-controlled diffusional creep, with contributions from both shear (τ_i) and normal stresses (σ_i) acting on the interface, with the sliding strain rate $\dot{\gamma}_i$ being given by :

$$\dot{\gamma}_i = \frac{4\delta_i D_{i0} \Omega}{kTh^3} \left[\tau_i + 2\pi^3 \left(\frac{h}{\lambda} \right)^3 \sigma_i \right] \exp \left[- \frac{Q_i}{RT} \right] \quad (1)$$

where δ_i is the thickness of the interface, Q_i and D_{i0} are the activation energy and frequency factor, respectively, for interfacial diffusion, Ω is the atomic volume of the diffusing species (i.e., film material), λ and h are the topographical periodicity and roughness, respectively, of the interface, and k , R and T are the Boltzmann's constant, gas constant, and the absolute temperature, respectively. Clearly, whereas the shear stress τ_i is the primary driving force for interfacial creep, the normal stress σ_i also has a contribution which depends strongly on the interfacial roughness parameter h/λ . A compressive (negative) σ_i would result in a threshold behavior and slow the rate of sliding, whereas a tensile (positive) σ_i would increase the effective stress at the interface, and hence enhance the sliding rate. Finally, since the sliding rate is

inversely proportional to h^3 , a smoother interface would be expected to slide more readily. Thus, smooth interfaces with a shear and a normal tensile stress acting on them would be the most susceptible to sliding.

Since significant interfacial shear stresses only exist near the edges of a thin film, interfacial sliding is an edge-effect, and as such, can be ignored for large-area films. However, with decreasing lateral film dimensions (e.g., in electronic applications where line widths are at the sub-micron level) these effects are likely to become important, particularly since the interfaces involved are very smooth and the interfacial shear stress is often augmented by normal tensile stresses (peeling stress) acting near the film edges.

3. Experimental Approach

An array of nominally 250 nm thick, 6 μm square pure Al films were deposited by thermal evaporation on to a Si (100) wafer utilizing a Ni mask. The polished surface of the Si wafer was cleaned prior to film deposition in accordance with standard micro-electronics practice. During deposition, the substrate temperature was maintained at 428 K, and the deposition rate was about 20 nm/min. The samples were subsequently annealed at 623 K for 15 min prior to removal of the Ni masks in order to promote diffusion-bonding at the interface, and to stabilize the film-microstructure. After removing the Ni masks, the samples were subjected to 5 thermal cycles from 293K to 623 K in a vacuum furnace at a pressure of $\sim 5.0 \times 10^{-7}$ Torr. During thermal cycling, the ramp-up rate was ~ 20 K/min, and the nominal cooling rate was ~ 2.5 K/min. Figure 1 shows a typical AFM image of the square Al films on a Si substrate on a $40\mu\text{m} \times 33\mu\text{m}$ scan area. Small scale scanning revealed that the surface roughness of the Si substrate is below 1 nm, suggesting that the interfaces between Al films and Si substrates is very smooth.

A pattern of parallel 1.4 μm wide Cu lines with a pitch of 2 μm was deposited on a (100) Si wafer via electroplating. The basic fabrication procedure consisted of lithographically defining the lines in a photo-resist coated on to the wafer, sputter-depositing a barrier layer of Ta and a seed layer of Cu, followed by Cu electro-plating, planarizing, and resist-stripping. Subsequently, the sample was annealed for 30 minutes at 673K to stabilize the Cu-grain structure, and then subjected to 5 thermal cycles from 293K to 723K in vacuum at nominal heating and cooling rates of 10K/minute. Figure 2 shows a typical AFM image of the Cu lines on Si substrate over a $10\mu\text{m} \times 5\mu\text{m}$ scan area.

To identify the deformation induced by thermal cycling, the cross-sectional profiles of the square Al films and Cu lines were measured before and immediately after thermal cycling by an AFM at room temperature in air. For the square Al films, the profiles were measured parallel to the square edge through the center of the square. For the Cu lines, the profiles were measured perpendicular to the line length far from the ends of the lines. For the Al films, the AFM measurements were carried out in non-contact mode, whereas for the Cu films, the contact mode was used in order to yield a better resolution. The lateral displacement resolution produced was estimated to be better than 15nm with the $20\mu\text{m}$ scan range used for the Al films, and 10nm with the $10\mu\text{m}$ range used for the Cu lines.

4. Modeling Approach

A plane-strain finite element (FE) model of a thin-film line on a Si substrate, with the model plane being normal to the line length, was developed in order to evaluate the film and interfacial stress and strain states associated with thermal cycling. Figure 3 shows a schematic of the model with the appropriate nomenclature. The model was built with the multi-purpose FE program ANSYSTM, utilizing 8-noded triangular solid elements for both film and substrate. The Si substrate was modeled as an isotropic elastic solid, whereas the metallic thin-film was represented as an isotropic elastic-plastic-creeping solid exhibiting temperature-dependent bilinear properties, and subject to dislocation creep via power-law (PL) and power-law breakdown (PLB). Since the FE model could account for only one creep law, a sinh-law was picked because dislocation creep prevails over a wide range of stress/temperature conditions, although it is realized that Coble creep is likely to be important at high temperatures [3]. Therefore, the

FEM analysis is expected to somewhat underestimate creep relaxation effects in the film at the higher end of the thermal cycle. Since temperature dependent thin film properties were not readily available, room temperature thin film properties were scaled to conform to the same temperature dependence as bulk polycrystalline elastic-plastic properties. For creep, data for bulk polycrystalline Al and Cu presented in ref. 11 were utilized. In the model, the interface was assumed to be perfectly bonded and non-sliding, because of the difficulty of incorporating the planar interfacial creep law into the FE program. For both Al and Cu, the film was assumed to be 100nm thick (t_f), and 5 μm wide (l_f), and the substrate was assumed to be 5 μm thick (t_s).

5. Results

5.1 Experimental

Figure 4 shows typical cross-sectional profiles of the Al films before and after 5 thermal cycles. Generally, after thermal cycling, the film-width close to the interface becomes larger and the slope of the film edges becomes shallower, indicating that (i) there is a gradient of plastic deformation along the through-thickness direction of the film, and (ii) more plastic deformation occurs close to the interface. Since there is statistical variation in the size of the film islands, we randomly measured the widths of about 70 square films and plotted the size distribution of the samples before and after thermal cycling in Figures 5a and 5b. All the values were measured at a height of 20 nm from the Si-Al interface. By fitting the histograms to a Gaussian distribution, it can be observed that the mean of the distribution (solid lines in Figure 5b) moves to a higher value after thermal cycling. Prior to thermal cycling, the edges of the square islands of Al-film were found to vary within a standard deviation (2σ) of $\pm 0.35\mu\text{m}$ from the mean of $5.99\mu\text{m}$. Following cycling, the mean shifted to $6.20\mu\text{m}$, with a 2σ value of $\pm 0.30\mu\text{m}$. It is believed that the difference of $\sim 0.2\mu\text{m}$ in the mean value arises due to plastic deformation of the film, induced by thermal cycling. The average lateral strain of the square films is $\sim 3.3\%$. After subtracting the elastic strain induced by residual tensile stresses, the plastic deformation of the films is estimated to be about 3%.

Figure 6 shows typical profiles of the Cu lines prior to, and following the first through fifth cycle. Contrarily to what is observed for Al films, the electroplated Cu lines are observed to shrink with progressive cycling, with the vertical profile of the film edges becoming sharper (i.e., less sloped). The histograms in Figure 7 show the line-width distributions 20nm from the interface at different stages of cycling. The mean of the distribution decreased from $1.429\mu\text{m}$ in the uncycled state to $1.294\mu\text{m}$ after the 5th cycle. The standard deviations of the width measurements ranged from 0.013 to $0.022\mu\text{m}$, well below the measured change in line width due to cycling. Figure 8 shows the change in width with progressive cycling. It is observed that the line width decreases almost linearly till the third cycle, after which the rate of change of width becomes slower. Presumably, the ratcheting down of the line width will saturate at a finite number of cycles, beyond which the line width would remain stable. Figure 8 also shows that corresponding to the decrease in line width, there is an increase in the line thickness (or height) during cycling. This increase in thickness is associated with the requirement to maintain volume constancy during plastic deformation of the lines.

5.2 Modeling

Figure 9 shows the computed stress distribution along the film width in an unpassivated Al film following cooling to ambient after annealing at 644K. Figure 9a plots the in-plane normal stress σ_{xx} very close to the interface ($y/t_f \approx 0.02$), whereas Figure 9b shows the interfacial shear stress τ_i at the interface ($y/t_f = 0$). All the stresses have been normalized by the elastic misfit stress σ_o , which is given by :

$$\sigma_o = \frac{(\alpha_s - \alpha_f) \Delta T}{\left(\frac{1 - \nu_f}{E_f}\right) + \left(\frac{1 - \nu_s}{E_s}\right)} \left(4 \frac{t_f}{t_s}\right) \quad (2)$$

where the subscripts f and s represent the film and the substrate, respectively, α , ν , E and t represent the coefficient of thermal expansion, Poisson's ratio, Young's modulus and thickness, respectively, and ΔT is the temperature range of cooling. It is apparent from Figure 9a that with a decrease in film width relative to film thickness (i.e., with increasing t_f/l_f), the in-plane normal stress decreases, but varies over a greater proportion of the film width. Whereas for $t_f/l_f=0.002$, σ_{xx} is nearly constant throughout the film width except right at the edge, for $t_f/l_f=0.5$, σ_{xx} varies throughout the film width. Since the interfacial shear stress τ_i is nominally proportional to the first derivative of σ_{xx} with respect to x , it is observed from Figure 9b that τ_i is zero throughout most of the film width for $t_f/l_f=0.002$, but becomes non-zero over a larger proportion of the film width as t_f/l_f increases. In general, τ_i is maximum at the film edge ($2x/l_f = 1$), and decreases with increasing distance from the edge. Figure 9b also shows that in addition to a large interfacial shear stress that exists near the film edges, there is a normal tensile (or peeling) stress σ_{yy} , which is large at the film edge, and decreases rapidly on moving away from the edge. It is further observed that this normal interfacial stress increases with decreasing film width (or increasing t_f/l_f). As discussed in section 3, τ_i and σ_{yy} together provide the impetus for interfacial sliding near the film edges. Since both these quantities are larger for smaller t_f/l_f , a narrower film is expected to display a greater degree of interfacial sliding.

Figure 10 shows the computed variation of the maximum in-plane film stress, at $2x/l_f = 0$ and $y/t_f = 0.5$ (i.e., at the centerline of the sample and mid-plane of the film), during thermal cycling for a pure Al film on Si, following initial cooling from the annealing temperature. Also shown on the same plot are the von-Mises (VM) creep and plastic strains at the same location. It is observed that the film stress starts from a large tensile value, which is rapidly relieved upon heating to $\sim 350\text{K}$, beyond which compressive stresses build up within the film. Around 380K , the compressive stresses in the film start getting relieved because of creep processes, resulting in a knee in the plot. Commensurately, the VM creep strain is observed to increase rapidly. During cooling, tensile stresses build up, first slowly because of creep, and then rapidly as creep processes decelerate. This is reflected by the decreasing V-M creep strain, suggesting creep in the opposite direction. Finally, around 350K , the tensile stresses become large enough to cause some yielding of the film, as reflected by an increase in the V-M plastic strain.

For clarity, it is useful to inspect the in-plane plastic and creep strain distributions (ϵ_{xx}^{pl} and ϵ_{xx}^{crp}) within the film at 623K (end of heating segment) and 300K (end of cooling segment). Figure 11 shows these strain distributions close to the film-edge. It is apparent that at 623K , the cumulative ϵ_{xx}^{pl} is in tension in most of the film (away from the edge), but the cumulative ϵ_{xx}^{crp} is in compression. It should be realized that the plastic strain was induced during initial cooling from the annealing temperature, and not during the thermal cycle. The creep strain, on the other hand, is induced entirely during cycling. So a net compressive inelastic strain is induced in the film during heating to 623K , most of it due to creep. During subsequent cooling, substantial tensile creep occurs, leaving only a small negative creep strain at 300K . Concurrently, a large tensile plastic strain is induced at the lower temperatures, resulting in a net tensile inelastic strain after 1 complete cycle. This is consistent with Figure 10, from which it may be inferred that during one complete thermal cycle, the net plastic strain is tensile, and the net creep strain (which is tensile up to $\sim 350\text{K}$, compressive from 350 to 623K , and tensile again during cooling from 623 to 300K) is slightly compressive, resulting in a net tensile inelastic strain at the end of the cycle.

Despite the net tensile inelastic strain, the footprint of the film is not expected to change in the absence of interfacial sliding. The induced inelastic strains serve mainly to relax the film stresses, and cause a change

in the film profile near the edge, as evident in Figure 11. Figure 12 shows the computed profiles of the right edge of the Al film at different stages of heating and cooling during the thermal cycle. Since interfacial sliding was not accounted for in the model, the observed changes in film width during cycling are related to associated changes in substrate dimensions at different temperatures. Because of the built-in stress state at ambient temperature, the film starts with a right-edge profile which slopes inward from the interface to the top. Upon heating (e.g., to 478K), as the film attempts to expand more than the substrate, the edge profile becomes steeper, and becomes almost vertically straight at 623K. Upon cooling, the initial slope is regenerated, and the film-edge returns to its original location. Only a small change in the edge-profile is observed in association with film plasticity near the edge. Figure 13 shows the distribution of τ_i near the edge of the Al film at various temperatures. Clearly, as the in-plane film stress transitions from tensile to compressive, the sense of the shear stress changes. At 300K, σ_{xx} is tensile and the sense of τ_i is such that it would make the film-edge move outward (i.e., towards larger $2x/l_f$ values) if sliding were allowed. At 478K during heating, on the other hand, σ_{xx} is compressive, and the prevailing sense of τ_i would make the film-edge move inward (towards smaller $2x/l_f$ values) with sliding occurring in the opposite direction. However, since τ_i is negative over the majority of the thermal cycle, if interfacial sliding were to occur, the film-edge immediately adjacent to the interface would be expected move outward relative to its initial position, resulting in an enlargement of the film-footprint on the substrate. This, in addition to the slight reduction of the edge-slope after one complete cycle (Figure 12), is consistent with experimental observations on Al-Si, as noted earlier.

Figures 14 through 17 show the equivalent plots for electroplated Cu on Si. The Cu is assumed to be stress-free at ambient temperature, since electroplated Cu has been observed to be nearly-stress free immediately following annealing [12]. As observed in Figure 14, even though the in-plane film stress starts at zero, it ratchets up and settles at a small positive value after one cycle. Following the first cycle, though, the stress does not ratchet up significantly any more. As in the case of Al, during heating, the stress builds up to a significant compressive value before relaxation via creep and plasticity occurs. Unlike in Al, however, even at the high temperature end of the cycle, the stress is not completely relieved, and the film remains in significant compression. During cooling, the compressive stress is relieved, and a tensile stress builds up, rapidly at first, and more slowly subsequently as the film undergoes plastic yielding. From the associated VM plastic strain plot, it is noted that unlike in the case of Al, the Cu film deforms by plastic yielding during heating (between 450 and 723K) as well as during cooling (below 400K).

Figure 15 shows the distribution of ϵ_{xx}^{pl} and ϵ_{xx}^{crp} close to the edge of the Cu film at the ends of the heating and cooling segments of the thermal cycle (723K and 300K). Since the film is stress-free prior to cycling at 300K, and is in deep compression at 723K (see Figure 14), both ϵ_{xx}^{pl} and ϵ_{xx}^{crp} are in compression through most of the film away from the edge. During subsequent cooling, tensile creep occurs, but a significant negative creep strain is left at 300K. Concurrently, a small tensile plastic strain is induced at the lower temperatures, but the net inelastic strain after 1 complete cycle is still fairly large and compressive. This is consistent with Figure 14, from which it may be inferred that compressive creep contributes a large proportion of the inelastic strain during one complete cycle, resulting in a net compressive inelastic strain.

Again, since interfacial sliding is not allowed by the model, the compressive inelastic strain should not alter the footprint of the film on the substrate, although it causes a change in the edge profile of the film. Figure 16 shows the profile of the right edge of the Cu film at different stages during the thermal cycle. Because of the absence of stress at the starting temperature, the film starts out with a vertical right-edge profile. Upon heating, the film-edge profile begins to slope outwards from the interface to the top, the slope becoming shallower with increasing temperature. Upon cooling, the edge-slope becomes steeper, and eventually settles at a small but finite value away from the vertical. Interestingly, the footprint of the film on the substrate appears to be significantly smaller at the end of the cycle, although interfacial sliding

was not accounted for in the model. This is attributable to the accommodation of compressive inelastic deformation of the film by elastic deformation of the substrate. This point is discussed further in section 6.

Figure 17 shows the distribution of τ_i near the edge of the Cu film at various temperatures. σ_{xx} is compressive during the entire heating segment and the associated positive τ_i would tend to make the film-edge move inward (towards smaller $2x/l_f$) if sliding were allowed. This trend continues even during the cooling segment till σ_{xx} becomes tensile around 550K, below which τ_i assumes a small negative value and tends to make the interface slide to the right. Overall though, if interfacial sliding could occur, the sense of τ_i over most of the thermal cycle would result in a net shrinkage of the film-footprint on the substrate, with the film edge moving inward. Once again, this is consistent with the trends observed experimentally on the Cu-Si sample.

6. Discussion

As noted above, the model showed that the Cu film displays an apparent footprint change even though interfacial sliding was not allowed. This is primarily attributable to the large net inelastic compressive deformation of the film during a complete thermal cycle, and the associated inability of the film stress to return to its starting value, as noted in Figure 15. Since the film ends with a tensile stress despite starting out stress-free, the substrate ends up with a compressive stress, and hence is elastically compressed at the end of the cycle relative to its starting state. This contraction of the substrate following cycling is responsible for the contraction of the line width apparent in Figure 16. Thus, a ratcheting of the stress state would typically be associated with an apparent change in line footprint, even when interfacial sliding does not occur. However, it should be noted that in the model, our substrate was only $5\mu\text{m}$ thick, and therefore, would be expected to display significantly greater contraction than real Si substrates, which are typically $500\text{-}700\mu\text{m}$ thick. As observed in Figure 16, the displacement of the film edge after one cycle is $\sim 0.04t_f$, which amounts to a footprint change of about 8nm. In the experiment, the Si wafer was $\sim 725\mu\text{m}$ thick, and therefore, apparent changes in film footprint due to elastic deformation of the substrate would be much less than 8nm, and hence indiscernible in the AFM. Since we observe a mean film shrinkage of $\sim 47\text{ nm}$ after the first cycle, and $\sim 135\text{nm}$ after the fifth (Figure 7), this must be due to interfacial sliding.

Because of the paucity of lattice dislocations and the difficulty of dislocation glide in thin films [1], the yield strength of thin films is usually high, and plastic deformation via dislocation glide at low temperatures is likely to be limited during thermal cycling. The dominant mechanism of plastic deformation of the thin film is therefore believed to be creep/stress relaxation. Indeed, Cu films on Si have been noted to creep at temperatures as low as 333K during thermal cycling [3] whereas Al films on Al_2O_3 have been thought to creep at even lower temperatures [13]. This is also borne out by the FEM results presented above, even though accurate temperature-dependent yield strength and creep data for thin films were not available for the model, and diffusional creep effects were ignored (which would have the effect of overestimating plastic strains and underestimating creep strains). In practice, therefore, creep effects are expected to be even more accentuated during thermal cycling than the FEM results would suggest. If interfacial sliding were not allowed, these large creep strains would simply result in stress relaxation of the film, with no discernible dimensional change. However, if interfacial sliding is allowed to occur, permanent relative change between the dimensions of the metal film and the Si substrate at the interface would be expected, as observed here experimentally. It is therefore believed that near the edges of the film, creep relaxation of the film is accommodated by interfacial sliding due to the presence of interfacial shear stresses, thereby allowing the film-dimensions to change. Since the permanent differential strain measured in the present work is $\sim 3\text{-}8\%$, which is much larger than the differential thermal expansion of the Al or Cu relative to Si over the entire test temperature range, it is inferred that the observed plastic strain accrues cumulatively during thermal cycling due to continuous stress and temperature revision. This

is consistent with Figure 7, which clearly demonstrates the cumulative nature of interfacial sliding displacement.

From the experimental results, it is interesting to note that the change in the Cu-line width after 5 cycles amounts to an average plastic strain of ~8%, which is significantly larger than the 3% plastic strain observed in the much wider Al films. This is despite the fact that the net inelastic strain induced in Cu during thermal cycling is on the same order (or somewhat smaller) as those in Al (compare Figures 10 and 14). This is consistent with the notion that interfacial sliding occurs only near the edges of the film where the shear stresses are significant. The Cu lines, being significantly narrower than the Al films in the present work, allow interfacial sliding to occur over a larger fraction of the line-width than the Al films. Since interfacial sliding is necessary to accommodate differential deformation of the film and Si, the Cu line shows a larger proportionate change in width than the Al films.

It was noted in the experiments that the edge-profile of the Cu line became steeper during cycling, as the Cu lines shrank. The model, however, showed that an originally vertical edge-profile developed a slope during cycling. However, these observations not inconsistent when the nature of the slopes are taken into account. In the model, an originally vertical profile became positively sloped (sloping outward from the interface to the film surface, or acute angle θ between film-edge and substrate surface). In the experiment, an originally negative edge-profile (sloping inward from the interface to the film surface, or obtuse angle θ between film-edge and substrate surface) tended to become vertical. Thus both model and experiment resulted in changes in the same direction, with θ decreasing due to cycling.

The shape change of films wherein the slope of the side faces changes after thermal cycling indicates that plastic deformation of the films is non-uniform in the through-thickness direction, and the typically assumed plane-stress condition is not valid at the microscopic level. Generally, following thermal cycling, the film is strained to a greater extent close to the film-substrate interfaces. This is primarily because the film has a through-thickness gradient of in-plane normal stresses, particularly near the edges. The in-plane stresses are typically largest at the interface, thereby allowing maximum creep/plasticity near the interface, as demonstrated by the strain distributions in Figures 11 and 15. Also, near the interface, film creep may be accommodated by interfacial creep, allowing the film dimensions to alter more.

From Figure 9, it is noted that with decreasing film aspect ratios (ratio of line-width to line-thickness), an increasingly larger proportion of the interface is subjected to shear stresses. Furthermore, significant peeling stresses (normal tensile stresses) may act on the interface near the film edges, the extent of the film subjected to such peeling stresses increasing with decreasing film aspect ratio. Indeed, as evident from Figure 9, for a film thickness of $0.1\mu\text{m}$ and a line width of $1\mu\text{m}$, interfacial shear stresses prevail over nearly the entire film width, and tensile peeling stresses exist over a distance of about 20% of the film-width from each film-edge. It is this combination of interfacial shear stress and the normal peeling stress near the edges of the film that is thought to drive interfacial sliding in order to accommodate creep deformation of the film. Clearly, the sense of the interfacial shear stress changes depending on the stress state of the film, as noted earlier for Al and Cu, allowing the film to either expand or shrink relative to the substrate. With an alteration of the in-plane stress state, the normal interfacial stress σ_i also changes sign, being tensile (peeling) for a tensile σ_{xx} , and compressive for a compressive σ_{xx} . Thus for equal magnitudes of the interfacial shear stress τ_i , the interfacial creep rate ($\dot{\gamma}_i$) should be greater when the film is in tension (since σ_i will augment τ_i ; eqn. 1), and slower when the film is in compression (since σ_i will result in a threshold stress; eqn. 1). The sliding rate is also enhanced by smoother interfaces (smaller values of h), which is why films deposited on smooth wafers (RMS roughness of $<1\text{nm}$, as in our experiments) display significant size changes. Interestingly, whereas a smoother interface tends to increase the sliding rate, it reduces the impact of the normal stress, since the effect of σ_i scales with $(h/\lambda)^3$.

Therefore, for very smooth interfaces, the effect of the normal stress may become quite small, resulting in little noticeable difference in the sliding rates for films in tension and compression.

In summary, the phenomenon of interfacial sliding-accommodated inelastic deformation of films would be expected to be more prominent for films with small lateral dimensions (e.g., narrow lines) and smooth interfaces. As the micro-electronic industry moves towards progressively larger-scale integration, dimensional stability of metallic lines is likely to become increasingly important, making it critical to understand the mechanisms and kinetics of interfacial sliding. In particular, it is necessary to develop methodologies to characterize the kinetics of interfacial sliding, and analytical techniques to account for these effects in modeling efforts. This is particularly important since with the advent of new generations of dielectric films with low elastic moduli (which may be more than an order of magnitude smaller than those of metallic films), the constraint traditionally imposed on the deformation of metal lines by stiff oxide passivations is no longer available.

7. Conclusions

The cross-sectional profiles of thin Al and Cu films on Si substrates were measured using AFM before and after thermal cycling under different conditions. It was observed that thermal cycling resulted in alteration of the lateral film dimensions, with the Al film expanding and the Cu lines shrinking relative to the substrate. Additionally, the edge profiles of the films were found to change because of through-thickness variations in the film stress and strain states, particularly near the edges. These changes were attributed to inelastic deformation of the film (mainly creep and some plastic yielding), accommodated by diffusively accommodated sliding at the interface. This sliding process is driven by interfacial shear stresses, and may either be augmented or ameliorated by interfacial normal stresses.

The evolution of stress and strain states within the film during thermal cycling were modeled using finite element analysis, and the observations were found to be consistent with the experimental trends. It was observed that large interfacial shear stresses usually exist near the edges of thin films, in association with in-plane film stresses which arise due to thermal expansion mismatch between the film and the substrate. It was further noted that with decreasing lateral film dimensions, interfacial shear stresses exist over a larger proportion of the film width. Since interfacial sliding is driven by these shear stresses, it is limited to regions very close to the film edge for large-area films. Therefore, for large-area films, dimensional changes due to interfacial sliding and film plasticity are negligible compared to film dimensions. However, with decreasing film dimensions, interfacial sliding, and hence changes in film dimensions, become more prominent.

The model also predicted slope changes of the film-edge profile due to through-thickness strain variations near the film edges, the predicted trends being consistent with experiments. Further, the model showed that the sense of the interfacial shear stress changes depending on whether the film is in in-plane tension or compression. This allows the direction of interfacial sliding to adjust itself so that the footprint of films subjected to a net tensile inelastic strain during thermal cycling can expand relative to the substrate, whereas films subjected to a net compressive inelastic strain can contract. This is consistent with the experimental observation that evaporated Al films expand whereas electroplated Cu films contract relative to the substrate during cycling. Finally, it was noted that decreasing interfacial roughness accelerates interfacial sliding, while reducing the contribution of interfacial normal stresses to the sliding kinetics.

Acknowledgements

This work was supported by the National Science Foundation, Division of Materials Research, under grant number DMR-0075281 with Dr. B. A. MacDonald as program monitor. MWC also acknowledges the support of the National Research Council Postdoctoral Associateship program. The authors are grateful to Dr. J. Molla of Motorola for supplying the Cu-Si samples.

References

1. W. D. Nix, *Metall. Trans.* 20A, 1989, p.2217.
2. F. R. Brotzen, *Int. Mater. Rev.* 39, 1994, 25.
3. M. D. Thouless, J. Gupta, and J. M. E. Harper, *J. Mater. Res.* 8, 1993, p.1845.
4. Y.-L. Shen and S. Suresh, *J. Mater. Res.* 10, 1995, p.1200.
5. M. W. Chen and I. Dutta, *Appl. Phys. Lett.*, 77, 2000, p. 4298.
6. R. Nagarajan, I. Dutta, J. V. Funn and M. Esmele, *Mater. Sci. Engg.*, A259, 1999, p. 237.
7. I. Dutta, *Acta Mater.* 48, 1055 (2000).
8. S. Yoda, N. Kurihara, K. Wakashima and S. Umekawa, *Metall. Trans.*, 9A, 1978, p. 234.
9. D. V. Zhmurkin and T. S. Gross, and L. P. Buchwalter, *J. Electronic Materials* 26, 791 (1997).
10. J. V. Funn and I. Dutta, *Acta Mater.* 47, 149 (1999).
11. H. J. Frost and M. F. Ashby, *Deformation Mechanism Maps*, Pergamon Press, Oxford (1982).
12. L. M. Gignac, K.P. Rodbell, C. Cabral Jr., P.C. Andricacos, P.M. Rice, R.B. Beyers, P.S. Locke and S.J. Klepeis, *Proc. Mat. Res. Soc. Symp.* vol. 564, 1999, p. 373.
13. Y.-L. Shen and S. Suresh, *Acta Mater.*, 44, 1996, pp. 1337-1348.

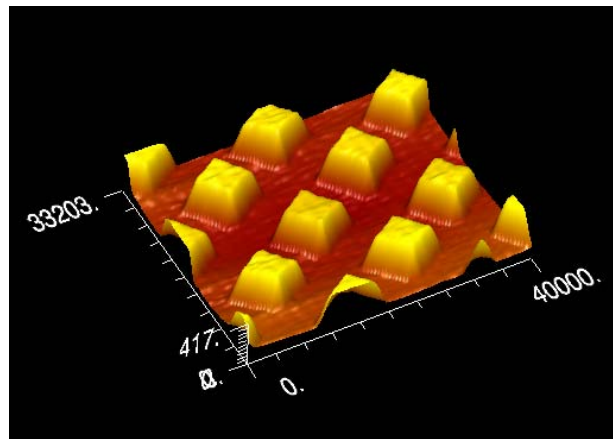


Figure 1 : AFM image of an array of square Al thin film islands on Si. Each island is nominally 250nm thick and has lateral dimensions of $6\mu\text{m} \times 6\mu\text{m}$.

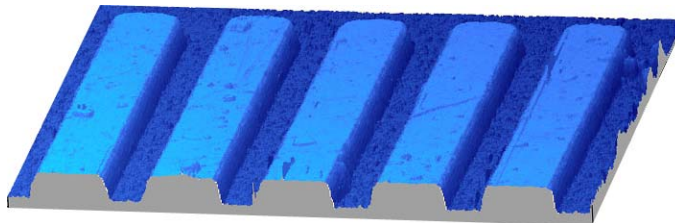


Figure 2 : AFM image of an array of parallel Cu lines on Si. The lines are nominally 250nm thick and $1.4\mu\text{m}$ wide.

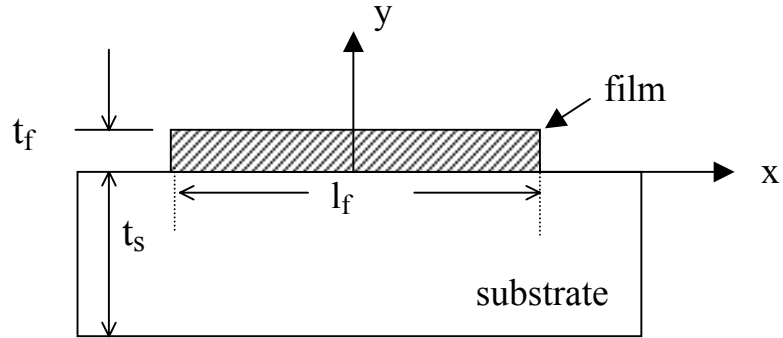


Figure 3 : Schematic of the film-substrate system with the appropriate nomenclature, used for the FE model. L_f is the film width, t_f the film thickness, and t_s the film thickness. Since the system is laterally symmetric, only half of the system (corresponding to positive x -values) was modeled. The film in the plane strain model represents a line running normal to the plane of the paper, with l_f representing the line-width.

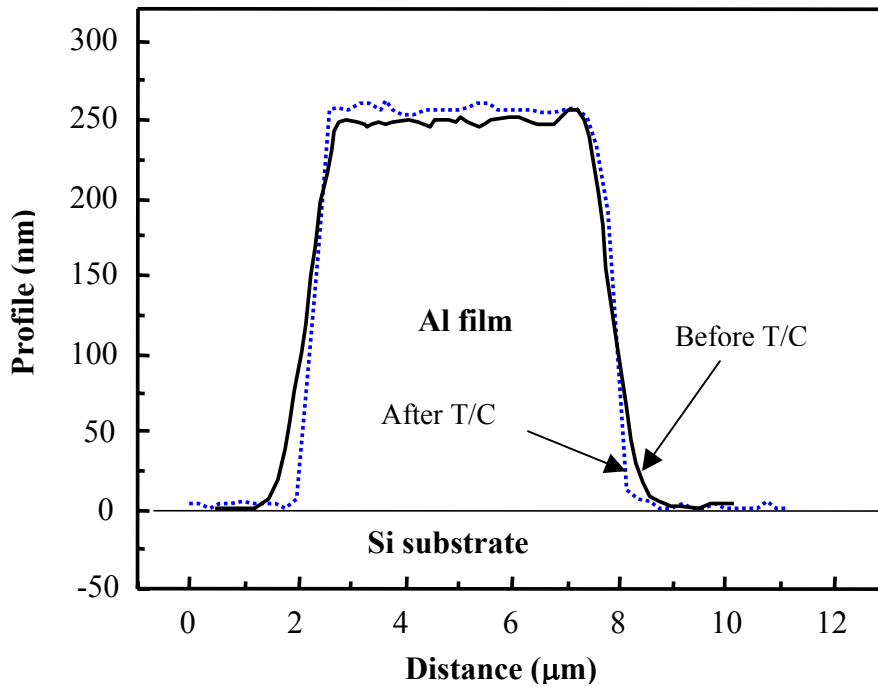


Figure 4 : Representative cross-sectional profiles of the square Al films before and after 5 thermal cycles from 293 to 623K.

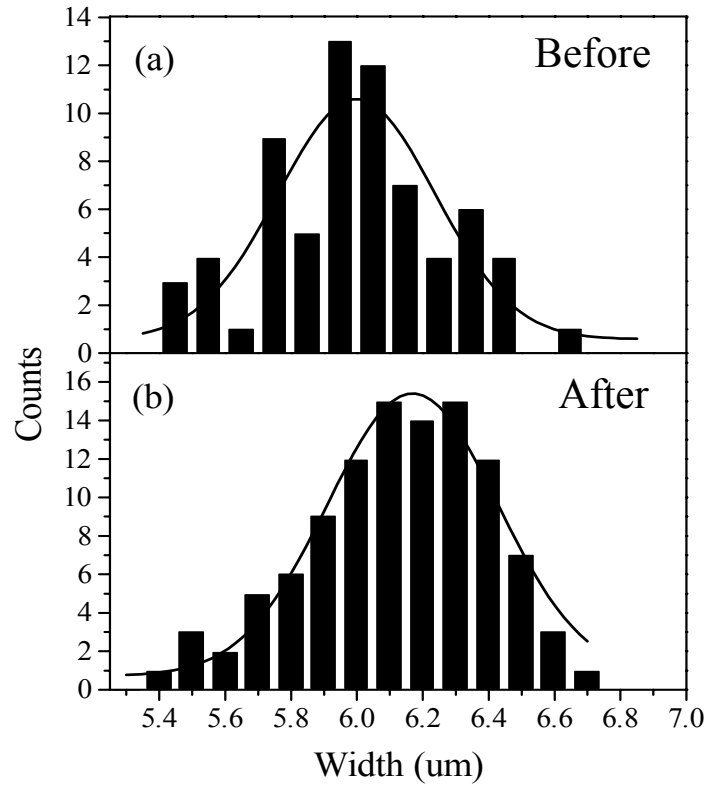


Figure 5 : Histograms and the associated Gaussian fits of the width distribution of the square Al films at a distance of 20nm from the interface; (a) before thermal cycles; and (b) after 5 thermal cycles.

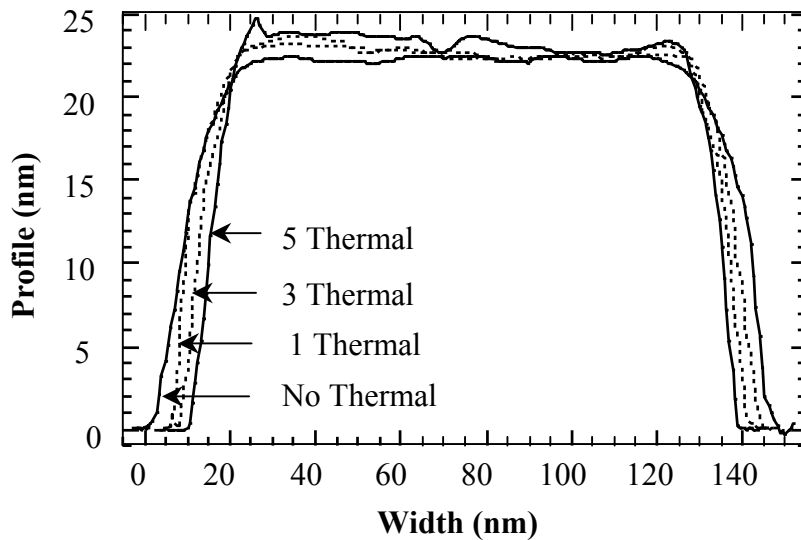


Figure 6 : Typical cross-sectional profiles of a Cu line at different stages of thermal cycling from ambient to 723K. The width of the Cu line is observed to decrease with increasing number of thermal cycles.

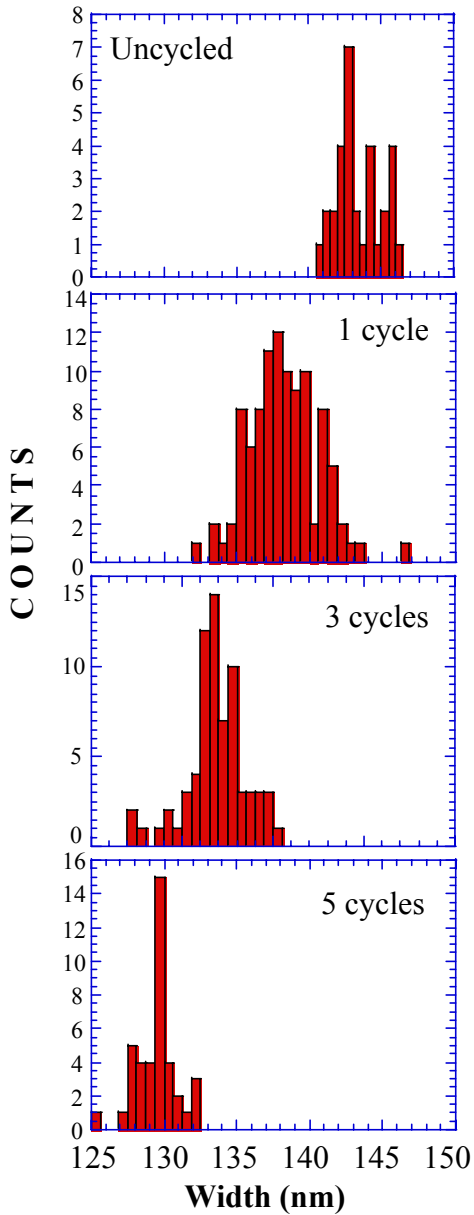


Figure 7 : Histograms of the width distribution of Cu lines at a distance of 20nm from the interface prior to thermal cycling, and following 1, 3 and 5 thermal cycles. The means and standard deviations of the distributions are as follows : (a) Before : 1429 ± 15 nm, (b) 1 cycle : 1382 ± 21 nm, (c) 3 cycles : 1317 ± 16 nm, and (d) 5cycles : 1296 ± 13 nm.

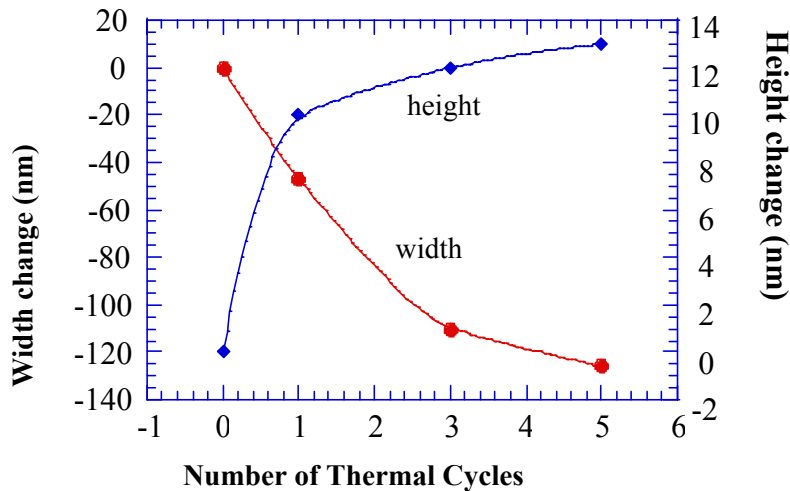
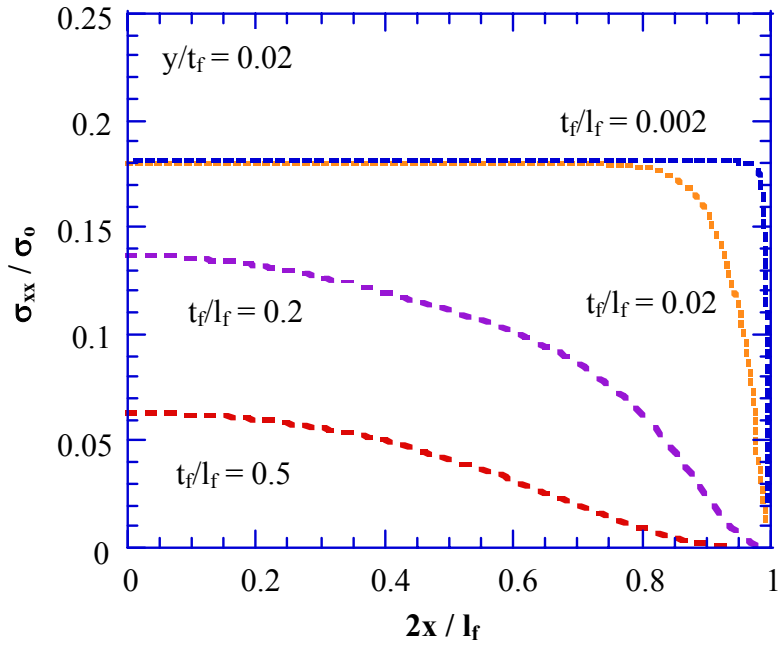
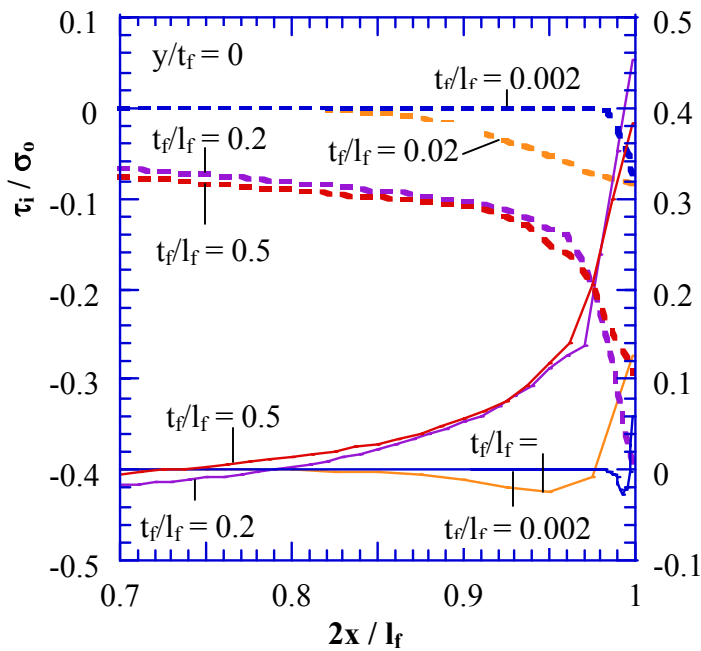


Figure 8 : Changes in Cu line width and line thickness plotted as a function of the number of thermal cycles.



(a)



(b)

Figure 9 : (a) Distribution of in-plane normal stress (σ_{xx}) along film-width for an Al film on Si at ambient temperature, following cooling from annealing temperature.

(b) Distribution of interfacial shear (τ_i) and normal ($\sigma_{i,yy}$) stresses along film-width for the same conditions. The dashed lines refer to τ_i , while the solid lines refer to $\sigma_{i,yy}$. All the stress distributions are shown for varying t_f/l_f values. The abscissa represents distance x along the film-width, normalized by half the film width $l_f/2$.

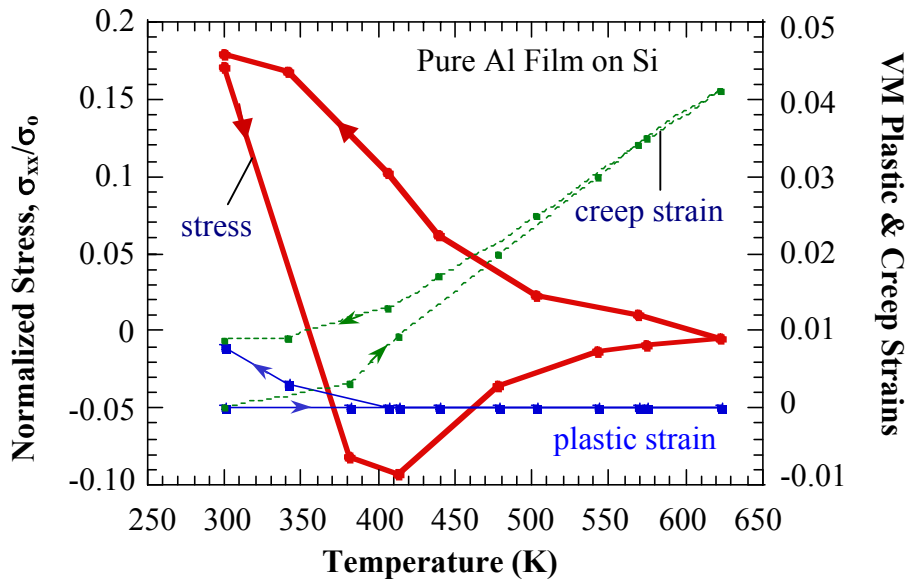


Figure 10 : Computed variation of σ_{xx} and the Von-Mises effective plastic and creep strains in an Al film during thermal cycling.

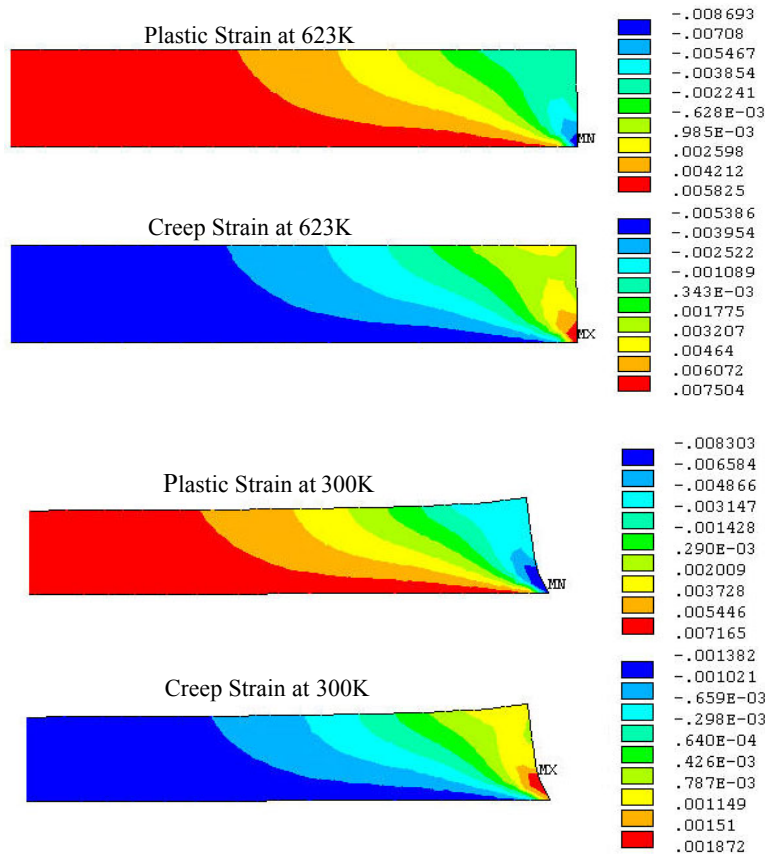


Figure 11: The distribution of in-plane plastic and creep strains near the edge of the Al film at the end of the heating segment (623K) and at the end of the thermal cycle (300K). The displacement scaling has been exaggerated to reveal changes in the edge profile associated with cycling. The middle of the film lies far away (beyond the picture) towards the left. All the contour plots have the same scaling, and the observed differences in size and location in the x-direction between the two temperatures are representative of reality.

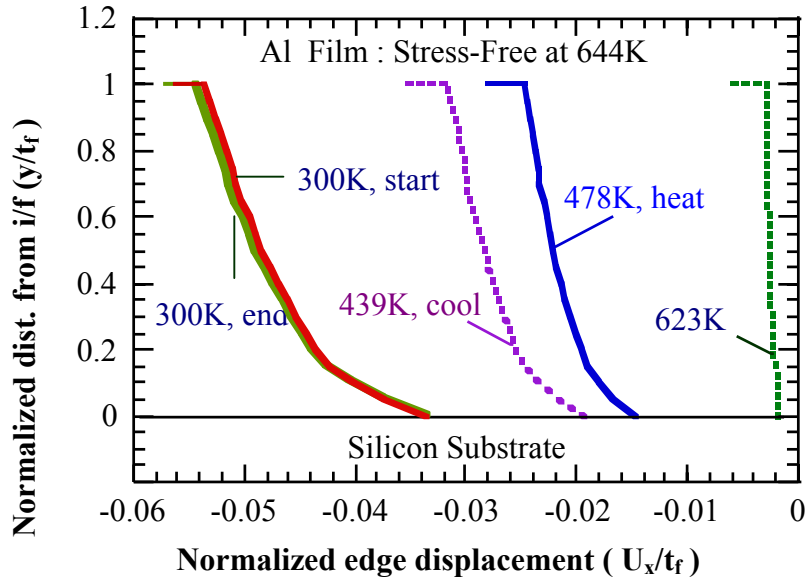


Figure 12: Computed profiles of the right edge of the Al film at different temperatures during heating and cooling. The horizontal line at the top of each edge-profile has been drawn in to delineate the film edge clearly, and do not represent the actual data.

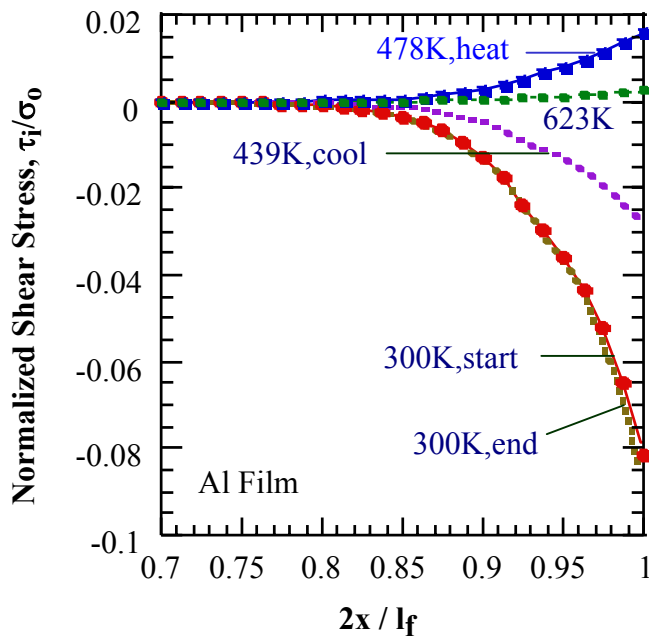


Figure 13: Distribution of interfacial shear stress τ_i close the edge of Al film at different temperatures during thermal cycling.

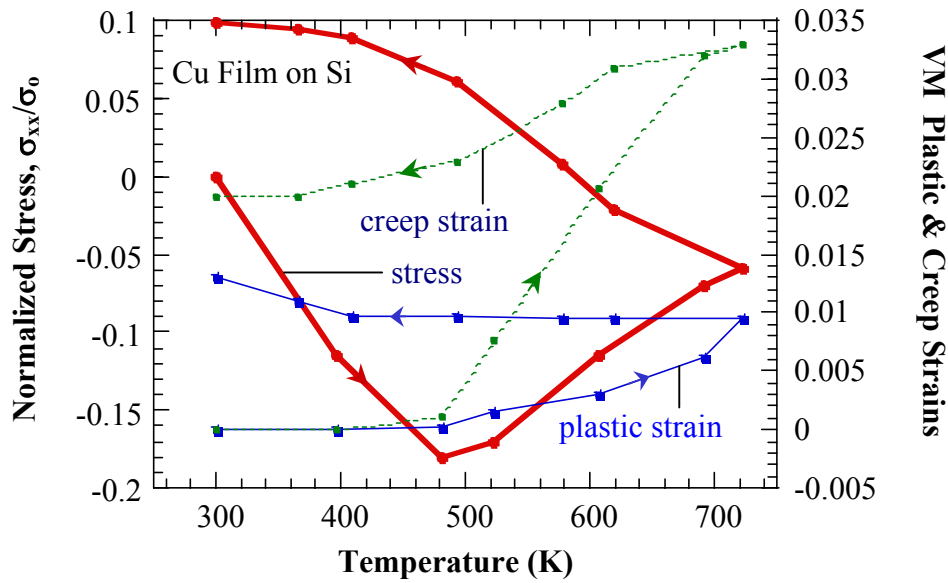


Figure 14 : Computed variation of σ_{xx} and the Von-Mises effective plastic and creep strains in an Cu film on Si during thermal cycling.

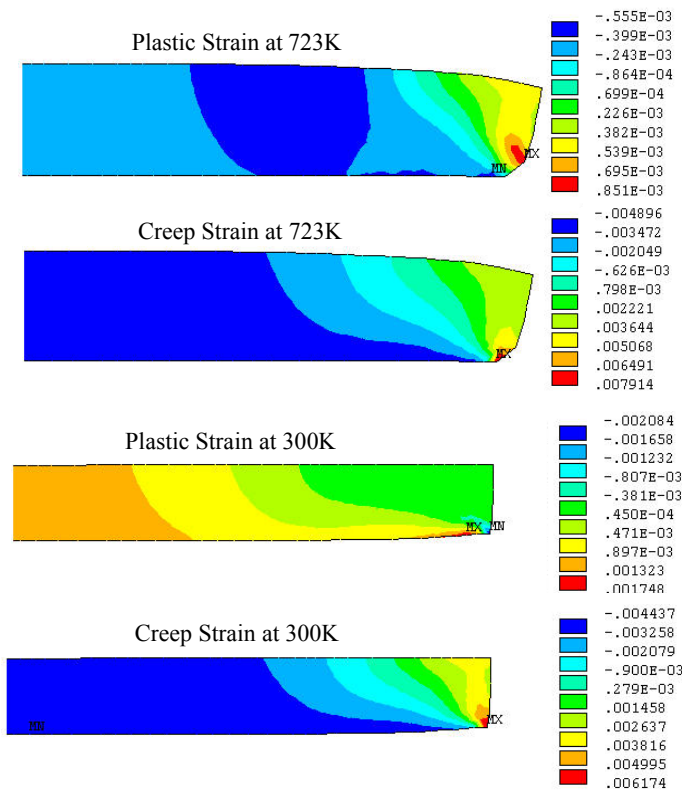


Figure 15: The distribution of in-plane plastic and creep strains near the edge of the Cu film at the end of the heating segment (723K) and at the end of the thermal cycle (300K). The displacement scaling has been exaggerated to reveal changes in the edge profile associated with cycling. The middle of the film lies far away (beyond the picture) towards the left. All the contour plots have the same scaling, and the observed differences in size and location in the x-direction between the two temperatures are representative of reality.

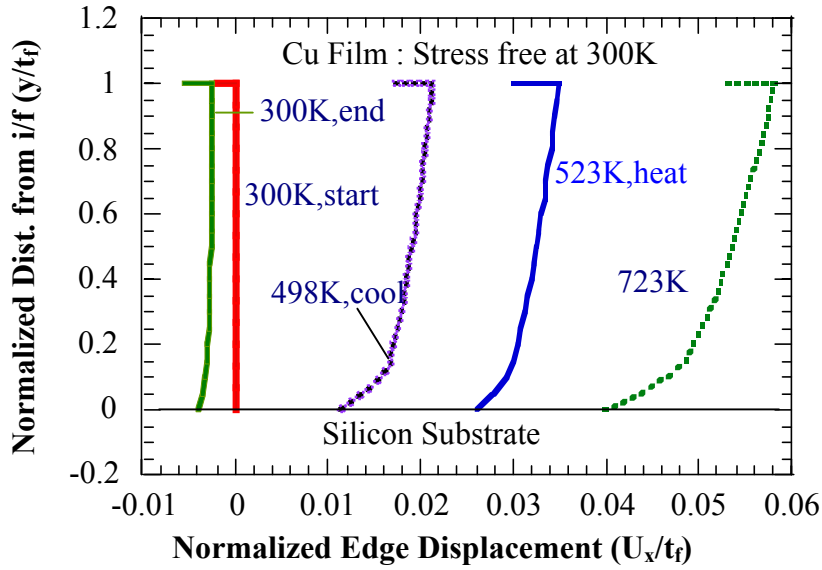


Figure 16: Computed profiles of the right edge of the Cu film at different temperatures during heating and cooling. The horizontal line at the top of each edge-profile has been drawn in to delineate the film edge clearly, and do not represent the actual data.

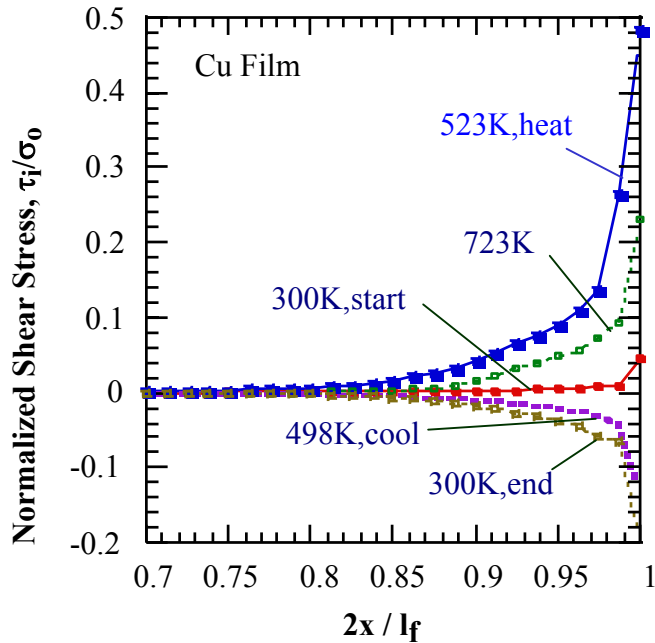


Figure 17: Distribution of interfacial shear stress τ_i close the edge of Cu film at different temperatures during thermal cycling.